A-ph 1703.01885

EVOLUTION OF GALACTIC OUTFLOWS AT $z \sim 0$–2 REVEALED WITH SDSS, DEEP2, AND KECK SPECTRA

YUMA SUGAHARA[1,2], MASAMI OUCHI[1,3], LIHWAI LIN[4], CRYSTAL L. MARTIN[5], YOSHIAKI ONO[1], YUICHI HARIKANE[1,2], TAKATOSHI SHIBUYA[1], AND RENBIN YAN[6]

[1]Institute for Cosmic Ray Research, The University of Tokyo, 5-1-5 Kashiwanoha, Kashiwa, Chiba 277-8582, Japan; sugayu@icrr.u-tokyo.ac.jp

[2]Department of Physics, Graduate School of Science, The University of Tokyo, 7-3-1 Hongo, Bunkyo, Tokyo, 113-0033, Japan

[3] Kavli Institute for the Physics and Mathematics of the Universe (WPI), The University of Tokyo, 5-1-5 Kashiwanoha, Kashiwa, Chiba 277-8583, Japan

[4] Institute of Astronomy & Astrophysics, Academia Sinica, Taipei 106, Taiwan (R.O.C.)

[5] Department of Physics, University of California, Santa Barbara, CA, 93106, USA and

[6] Department of Physics and Astronomy, University of Kentucky, 505 Rose St., Lexington, KY 40506-0057, USA

Submitted to ApJ

ABSTRACT

We study galactic outflows of star-forming galaxies at $z \sim 0$–2 based on optical spectra with absorption lines of Na I D, Mg I, Mg II, C II, and C IV. The spectra of galaxies at $z \sim 0$, 1, and 2 are taken from the large-survey data sets of SDSS DR7, DEEP2 DR4, and Erb et al. (2006a,b), respectively. To remove possible systematics of galaxy samples at different redshifts, we carefully construct large and homogeneous galaxy samples with similar stellar mass distributions. We stack the galaxy spectra in our samples, and perform the multi-component fitting of model absorption lines and stellar continua to the stacked spectra. We obtain the central ($v_{\rm out}$) and maximum ($v_{\rm max}$) outflow velocities, and estimate the mass loading factors (η) that are defined by the ratio of the mass outflow rate to the star formation rate (SFR). Because our optical spectra do not cover all of the absorption lines at each redshift, for investigating the redshift evolution, we compare outflow velocities at different redshifts with the absorption lines whose depths and ionization energies are similar. Na I D and Mg I at $z \sim 0$–1 (IE $\sim$ 5–8 eV) and Mg II and C II at $z \sim 1$–2 (IE $\sim$ 20 eV). We identify, for the first time, that the average value of $v_{\rm out}$ ($v_{\rm max}$) monotonically increases by 0.1–0.4 dex from $z \sim 0$ to 1 at the 3.0σ (4.9σ) significance levels and $z \sim 1$ to 2 at the 13.4σ (6.4σ) significance levels at a given SFR. Moreover, based on the absorption lines of Na I D at $z \sim 0$, Mg I at $z \sim 1$, and C II at $z \sim 2$, we find that the value of η increases from $z \sim 0$ to 2 by $\eta \propto (1+z)^{1.8\pm0.5}$ at a given halo circular velocity $v_{\rm cir}$, albeit with a potential systematics caused by model parameter choices. The redshift evolution of $v_{\rm out}$ ($v_{\rm max}$) and η are probably explained by high gas fractions in high-redshift massive galaxies, which is supported by recent radio observations. We obtain a scaling relation of $\eta \propto v_{\rm cir}^{a}$ for $a = -0.5 \pm 1.1$ in our $z \sim 0$ galaxies. This scaling relation agrees well with the momentum-driven outflow model ($a = -1$) within the uncertainty.

Keywords: galaxies: formation — galaxies: evolution — galaxies: ISM — galaxies: kinematics and dynamics

1. INTRODUCTION

collapse SNe (e.g., Larson 1974; Chevalier & Clegg 1985;

- Цель: оценить outflow по выбранным линиям поглощения Na I D, Mg I, Mg II, C II, and C IV. The spectra of galaxies at z = 0, 1, and 2 are taken from the large-survey data sets of SDSS DR7, DEEP2 DR4, and Erb et al. 2006a,b), respectively.
- Составленные выборки для z=0, 1, 2 имеют сходное распределением галактик по массам. Спектры складывались. Для оценки экв. ширины вычитались модельные звездные спектры.

- Stellar masses M are obtained by the fitting to the photometry (Kauffmann et al. 2003; Salim et al. 2007).
- SFRs within the fiber (SFRfiber) are measured from the extinction-corrected H emission-line flux, and
- total SFR are estimated by applying aperture correction with the photometry outside the fiber (Brinchmann et al. 2004).

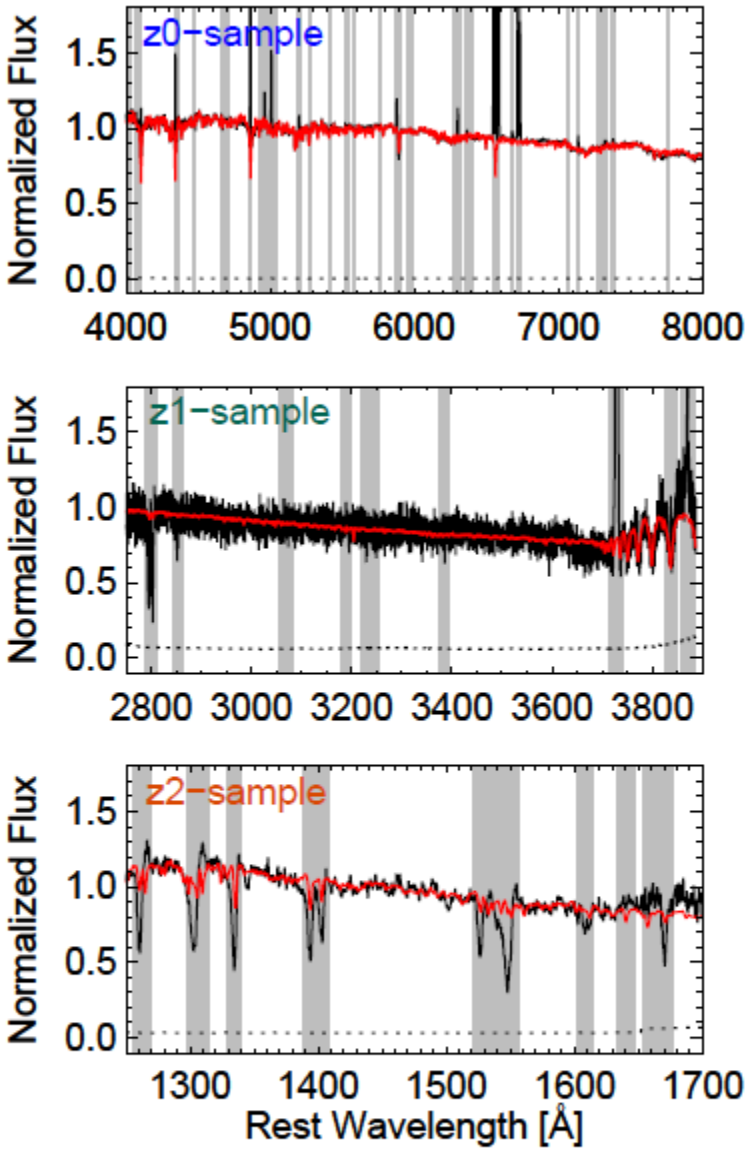

Figure 2. Examples of the stacked spectra (black line) and the best-fitt continuum models (red line). The spectra of the $z0$-, $z1$-, and $z2$-samples shown from top to bottom. The wavelength range shown in this figure is u for the stellar continuum fitting, except for the gray shading. The doted li denote 1σ uncertainties of the spectra.

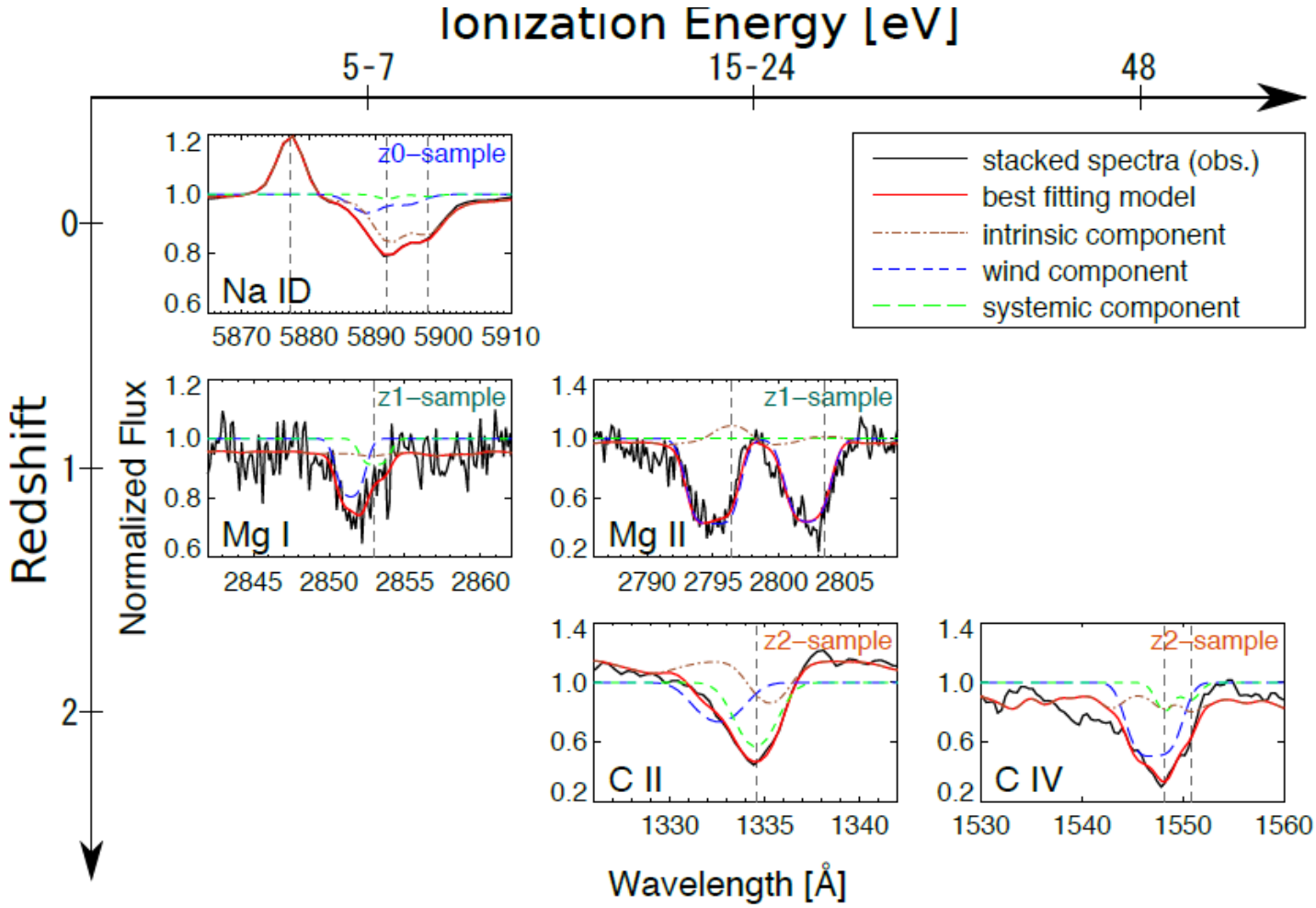

Figure 3. Examples of the stacked spectra around the absorption lines (black line). The red lines represent the best fitting models. The dot-dashed brown, dashed blue, and long-dashed green indicate the breakdowns of the lines for the intrinsic, wind, and systemic components, respectively. In this figure, the redshift (the ionization energy) increase from top to bottom (from left to right). The ions of the absorption lines are written at the bottom-left corner of the panels, and the samples are written at the top-right corner. The vertical dashed gray lines denote the rest-frame wavelengths of the absorption lines, except for the line at 5877.29 Å in the top-left panel, which represents the wavelengths of He I emission.

Table 1
Properties of the stacked spectra

sample	line	number[a]	z[b]	SFR[c] ($M_\odot$ yr^{-1})	M_*[d] ($M_\odot$)	v_{out}[e] (km s^{-1})	v_{max}[f] (km s^{-1})	η[g]
z0-sample	Na I D	125	0.063	0.44	10.1	144 ± 6	211 ± 21	2.1 ± 1.7
	Na I D	114	0.072	0.62	10.2	130 ± 5	218 ± 15	1.7 ± 1.0
	Na I D	118	0.079	0.74	10.3	138 ± 5	269 ± 12	2.1 ± 0.92
	Na I D	123	0.098	0.86	10.4	151 ± 15	301 ± 30	1.9 ± 1.1
	Na I D	133	0.12	1.0	10.5	146 ± 15	308 ± 31	1.7 ± 0.99
	Na I D	172	0.16	1.3	10.8	162 ± 15	353 ± 27	1.5 ± 0.79
z1-sample	Mg I	665	1.4	0.70	9.96	228 ± 35	504 ± 60	11 ± 7.5
	Mg I	395	1.4	0.92	10.3	166 ± 16	315 ± 69	2.5 ± 3.5
	Mg I	277	1.4	1.2	10.6	171 ± 20	395 ± 99	2.8 ± 4.4
	Mg II	665	1.4	0.70	9.96	161 ± 8	431 ± 20	3.9 ± 2.4
	Mg II	395	1.4	0.92	10.3	148 ± 9	452 ± 25	3.7 ± 2.5
	Mg II	277	1.4	1.2	10.6	203 ± 6	576 ± 21	3.5 ± 2.0
z2-sample	C II	25	2.2	1.4	10.3	439 ± 25	865 ± 25	15 ± 5.6
	C IV	25	2.2	1.4	10.3	429 ± 17	855 ± 17	19 ± 6.2

[a] Number of galaxies used for a composite spectrum.
[b] Median redshift
[c] Median star formation rate
[d] Median stellar mass
[e] Central outflow velocity defined in Section 4.1
[f] Maximum outflow velocity defined in Section 4.1
[g] Mass loading factor defined in Section 5.1

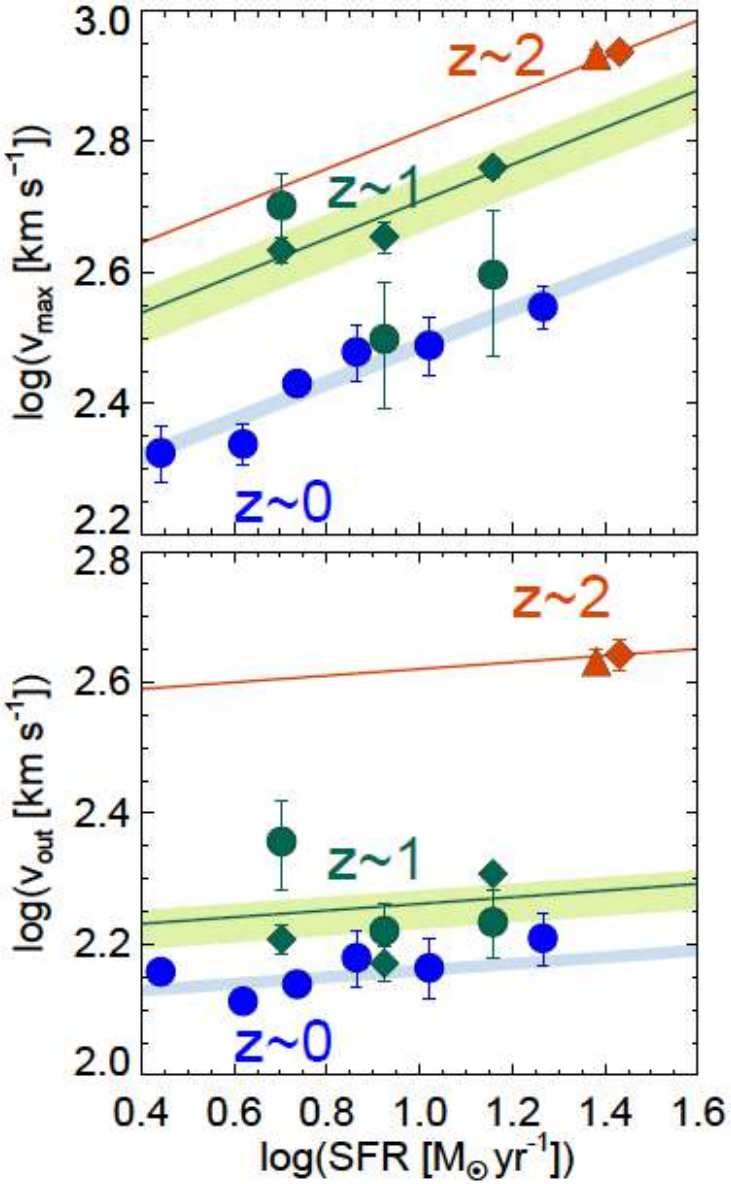

Figure 7. Same as Figure 4, but for the $z0$- (blue symbol), $z1$- (green s
bol), and $z2$- (red symbol) samples. Top: the maximum outflow velocitie
a function of SFRs. Each symbol corresponds to the elements of the abs
tion lines: Na I D (blue circle), Mg I (green circle), Mg II (green diamo
C II (orange diamond), and C IV (orange triangle). The circles, diamo

Результирующие соотношения

The redshift evolution of SFR is given by

$$\mathrm{SFR} \propto (1+z)^{2.8} \tag{16}$$

from the results of Speagle et al. (2014). In this study, we obtain $v_{\mathrm{out}} \propto (1+z)^{0.81\pm0.05}\mathrm{SFR}^{0.05\pm0.04}$, fitting the power-law functions to the results of Figure 7. Substituting Equation (16), we find

$$v_{\mathrm{out}} \propto (1+z)^{0.95\pm0.12}. \tag{17}$$

$$v_{\mathrm{max}} \propto \mathrm{SFR}^{0.28\pm0.05}.$$

- Скорость outflow (особенно максимальная) растет с SFR и z, особенно сильно между z=1 и z=2 (различие составляет 8.5 σ для V_{out})
- Mass loading factor η

Mass loading factor

$$\eta = \dot{M}_{\rm out}/SFR$$

$$\dot{M}_{\rm out} = \bar{m}_p \Omega C_f v_{\rm out} R N({\rm H}),$$

where $\bar{m}_p$ is mean atomic weight, R is the inner radius of outflows, and N(H) is the column density of hydrogen. where we use $\bar{m}_p = 1.4$ amu and $\Omega = 4\pi$ that is a case of a spherical outflow. We assume that R is the same as the effective radius which are obtained in the r_e–M_* relation of Shibuya et al. (2015).

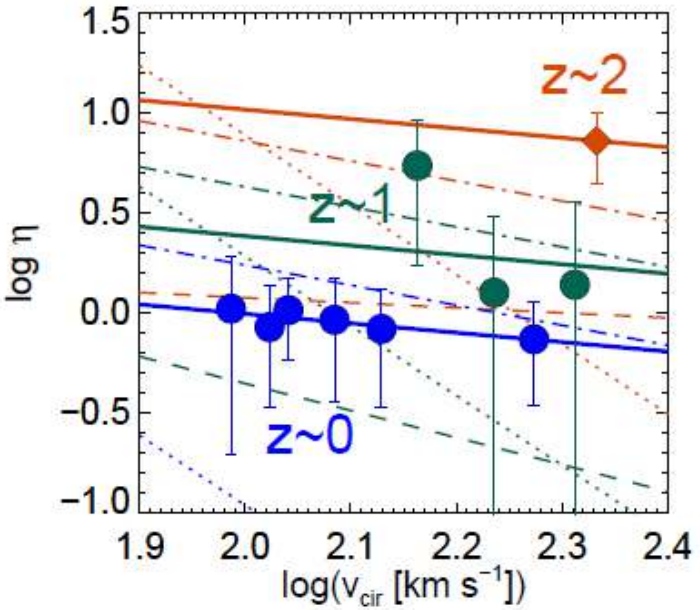

Figure 8. Mass loading factor as a function of $v_{\rm cir}$. The data points are the same as those in Figure 7. The colors of blue, green, and orange correspond to $z \sim 0$, 1, and 2, respectively. The solid lines denote the linear-square fitting results. The dot-dashed, dashed, and dotted lines indicate the models presented by Muratov et al. (2015), Barai et al. (2015), and Mitra et al. (2015), respectively.

A-ph 1703.02053

Galaxy Zoo: star-formation versus spiral arm number

Ross E. Hart,[1]★ Steven P. Bamford,[1] Kevin R.V. Casteels,[2] Sandor. J. Kruk,[3]
Chris J. Lintott,[3] Karen L. Masters[4]
[1]*School of Physics & Astronomy, The University of Nottingham, University Park, Nottingham NG7 2RD, UK*
[2]*Department of Physics and Astronomy, University of Victoria, Victoria, BC V8P 1A1, Canada*
[3]*Oxford Astrophysics, Department of Physics, University of Oxford, Denys Wilkinson Building, Keble Road, Oxford OX1 3RH, UK*
[4]*Institute for Cosmology and Gravitation, University of Portsmouth, Dennis Sciama Building, Portsmouth PO1 3FX, UK*

Accepted XXX. Received YYY; in original form ZZZ

ABSTRACT
Spiral arms are common features in low-redshift disc galaxies, and are prominent sites of star-formation and dust obscuration. However, spiral structure can take many forms: from galaxies displaying two strong 'grand design' arms, to those with many 'flocculent' arms. We investigate how these different arm types are related to a galaxy's star-formation and gas properties by making use of visual spiral arm number measurements from Galaxy Zoo 2. We combine UV and mid-IR photometry from GALEX and WISE to measure the rates and relative fractions of obscured and unobscured star formation in a sample of low-redshift SDSS spirals. Total star formation rate has little dependence on spiral arm multiplicity, but two-armed spirals convert their gas to stars more efficiently. We find significant differences in the fraction of obscured star-formation: an additional ~ 10 per cent of star-formation in two-armed galaxies is identified via mid-IR dust emission, compared to that in many-armed galaxies. The latter are also significantly offset below the IRX-β relation for low-redshift star-forming galaxies. We present several explanations for these differences versus arm number: variations in the spatial distribution, sizes or clearing timescales of star-forming regions (i.e., molecular clouds), or contrasting recent star-formation histories.

In this paper, the star formation and gas properties of spiral galaxies are compared with respect to spiral arm number. We use the visual classifications from Galaxy Zoo 2 (GZ2; Willett et al. 2013) to define samples of spiral galaxies differentiated by arm number (Hart et al. 2016). These are compared by combining estimates of SFRs measuring unobscured ultraviolet (UV) emission and obscured mid-infrared (MIR) emission.

Atomic gas fractions are also compared to investigate whether the presence of different types of spiral structure lead to deviations in star formation efficiency.

Полная выборка и под-выборки

Morphology	Full sample	M_*-limited	α70 detected
All	45192	25063	5570
Spiral	6333	3889	1792
$m = 1$	482	224	106
$m = 2$	3298	1953	859
$m = 3$	1263	805	391
$m = 4$	534	357	165
$m = 5+$	756	550	271

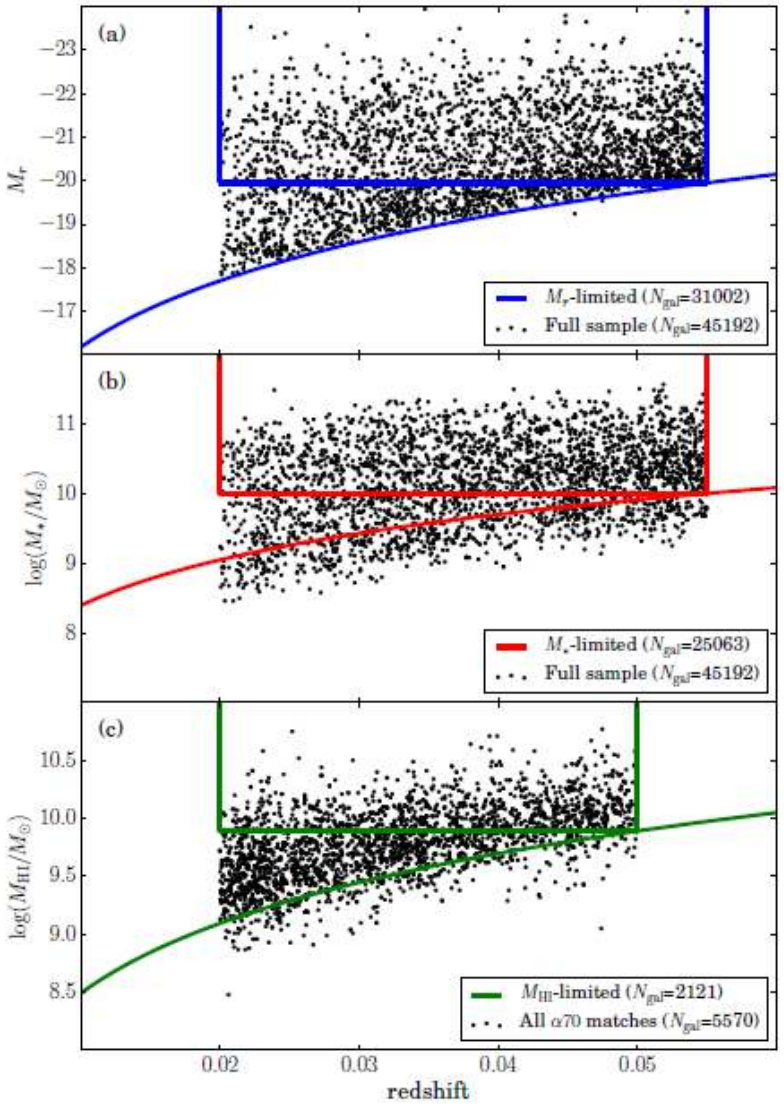

Figure 1. (a) Plot of absolute magnitude vs. redshift for the *full sample* of galaxies. The curved blue line indicates the luminosity limit as a function of redshift. Galaxies enclosed within the blue box make up the *luminosity-limited sample*. (b) Stellar mass distribution of the *full sample* vs. redshift. The curved line shows the calculated stellar mass completeness limit and galaxies. Galaxies in the red boxed region are included in the *stellar mass-limited sample*. (c) Gas mass vs. redshift for all galaxies matched in α70

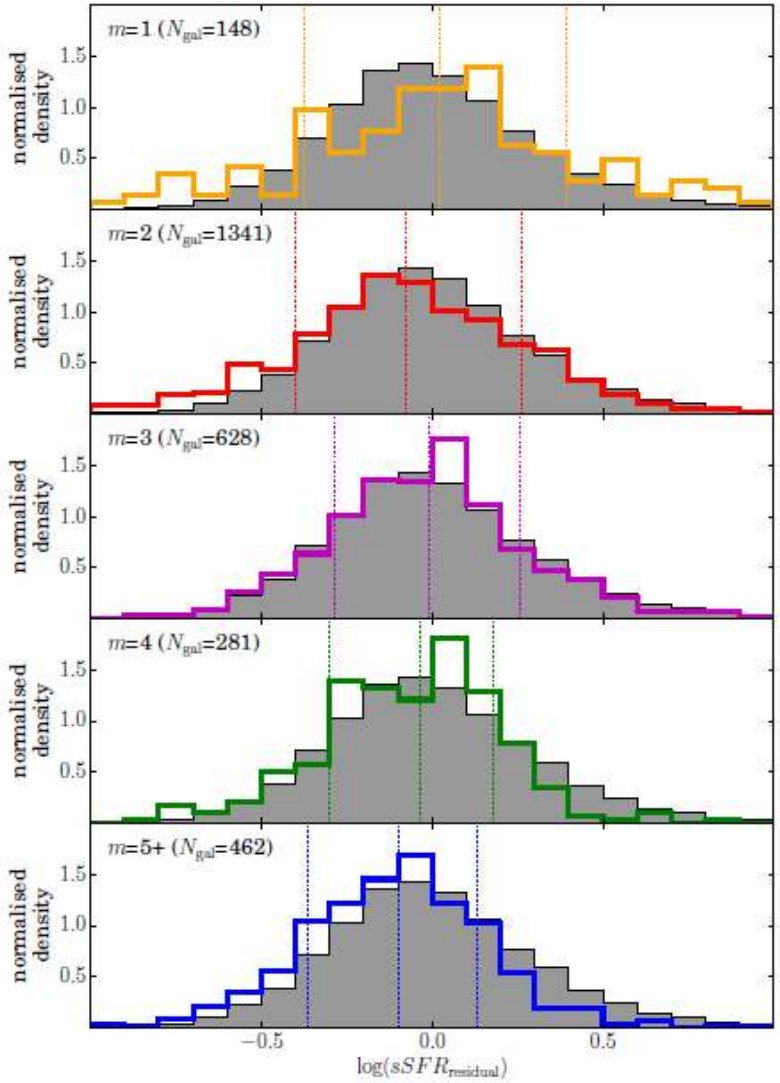

Figure 6. Residual sSFRs for each of the *arm number subsamples* taken from the *stellar mass-limited sample*, calculated using equations 7 and 8. The solid histograms show the distributions for each subsample, and the filled grey histograms indicate the same distributions for the entire sample of *star forming* galaxies for reference. The vertical dotted lines indicate the 16th, 50th and 84th percentiles.

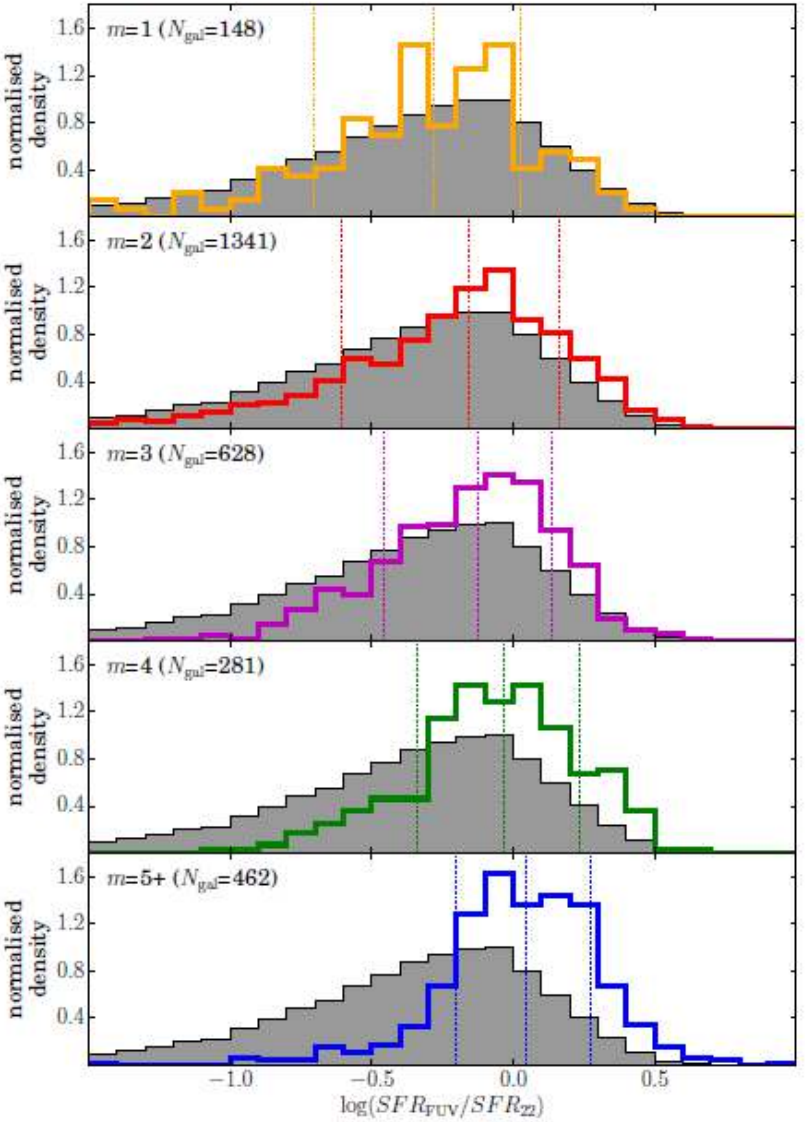

Figure 7. sSFRs measured in the FUV and MIR for the *stellar mass-limited samples*. The grey filled histogram shows the same distribution for all galaxies in the *stellar mass-limited sample*, irrespective of morphology. The vertical lines show the median, 16th and 84th percentiles for each of the *arm number subsamples*.

Как оценивалось HI deficiency?

(грубо до неприличия)

$$\log(M_{\rm HI}/M_*)_{\rm expected} = -0.70\log(M_*/M_\odot) + 6.61\ . \qquad (11)$$

The scatter in this relationship is 0.26 dex. One can now measure the HI deficiency using (Masters et al. 2012):

$$\log(M_{\rm HI}/M_*)_{\rm deficiency} = \log(M_{\rm HHI}/M_*)_{\rm expected} - \log(M_{\rm HI}/M_*)\ , \qquad (12)$$

where $\log(M_{\rm HI}/M_*)_{\rm expected}$ is given in Eq. 11. Galaxies with higher gas fractions than expected for their stellar mass have negative HI deficiency, and galaxies with low HI fractions have positive HI deficiency.

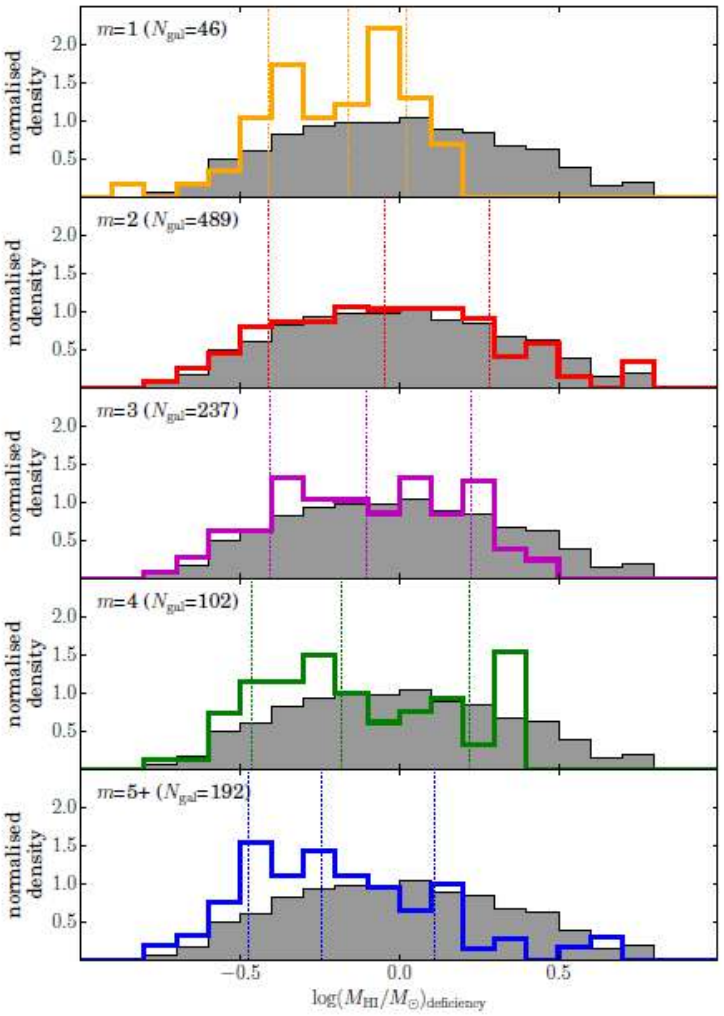

Figure 11. HI deficiency, calculated using equations 11 and 12, for each of the *arm number subsamples*. The underlying grey histograms show the distributions for all galaxies with detected HI, irrespective of morphology and the solid lines show the same distributions for all galaxies split by spiral arm number. Each HI detection is weighted by $1/V_{\rm max}$, and the vertical lines show the positions of the median, 16th and 84th percentiles for each spiral arm number. The dotted vertical lines show the median, 16th and 84th percentiles of each of the distributions.

Основные выводы

- For galaxies with reliable UV and MIR detections, sSFR has no significant dependence on spiral arm number.
- Spirals with different numbers of arms do have different levels of dust obscuration, with many-armed spirals having more UV emission from young stars unobscured by dust. The differences could be due to the relative distribution of star forming regions in galaxies with different spiral structure. In grand design spirals, the molecular clouds may be more concentrated in the dense arm regions. The consequent increase in dust obscuration may lead to a reduction in UV emission compared to that in the MIR.
- Two-armed spirals are more gas deficient than many-armed spirals, meaning they are more efficient at converting to stars.
- Two-armed spirals are also more likely to host bars, with 50 per cent having strong bars compared to only 20 per cent of many-armed galaxies.

TRIANGULUM II: NOT ESPECIALLY DENSE AFTER ALL

Evan N. Kirby[1], Judith G. Cohen[1], Joshua D. Simon[2], Puragra Guhathakurta[3], Anders O. Thygesen[1], Gina E. Duggan[1]

Accepted to ApJ on 2017 March 8

ABSTRACT

Among the Milky Way satellites discovered in the past three years, Triangulum II has presented the most difficulty in revealing its dynamical status. Kirby et al. (2015a) identified it as the most dark matter-dominated galaxy known, with a mass-to-light ratio within the half-light radius of 3600^{+3500}_{-2100} $M_\odot$ $L_\odot^{-1}$. On the other hand, Martin et al. (2016) measured an outer velocity dispersion that is 3.5 ± 2.1 times larger than the central velocity dispersion, suggesting that the system might not be in equilibrium. From new multi-epoch Keck/DEIMOS measurements of 13 member stars in Triangulum II, we constrain the velocity dispersion to be $\sigma_v < 3.4$ km s^{-1} (90% C.L.). Our previous measurement of σ_v, based on six stars, was inflated by the presence of a binary star with variable radial velocity. We find no evidence that the velocity dispersion increases with radius. The stars display a wide range of metallicities, indicating that Triangulum II retained supernova ejecta and therefore possesses or once possessed a massive dark matter halo. However, the detection of a metallicity dispersion hinges on the membership of the two most metal-rich stars. The stellar mass is lower than galaxies of similar mean stellar metallicity, which might indicate that Triangulum II is either a star cluster or a tidally stripped dwarf galaxy. Detailed abundances of one star show heavily depressed neutron-capture abundances, similar to stars in most other ultra-faint dwarf galaxies but unlike stars in globular clusters.

Keywords: galaxies: dwarf — Local Group — galaxies: abundances

Triangulum II- рекордсмен по DM?

- Это UFD –галактика
- Laevens et al. (2015) discovered Tri II. Its luminosity is just 450 $L_{\odot}$, and its 2D half-light radius is only 34 pc. Kirby et al. (2015a, hereafter K15a) measured its velocity dispersion from medium-resolution, multi-object spectroscopy to be $\sigma v = 5.1\ (+4.0\ -1.4)$ km s−1 from six stars. Martin et al. (2016) found that it increased to as much as 14 km s−1 in the outermost parts of the galaxy. Such a galaxy would almost certainly be out of dynamical equilibrium. If Tri II is in dynamical equilibrium, either measurement of the velocity dispersion would make it the most dark matter-dominated galaxy known.
- ПРОБЛЕМА В УЧЕТЕ ДВОЙНЫХ СИСТЕМ

- The only way to determine the binarity of most red giants in dwarf galaxies is multi-epoch spectroscopy to search for variability in radial velocity.
- The Deep Extragalactic Imaging Multi-Object Spectrograph is a medium- resolution spectrograph at the Nasmyth focus of the Keck II telescope.
- We matched the observed spectra to template spectra. We varied the radial velocity of the template spectra to minimize $\chi 2$. We also correcting for mis-centering in the slit by shifting the spectrum to ensure that telluric features, such as the Fraunhofer A and B bands, were at zero velocity.
- The data set contains 13 stars identified as members.

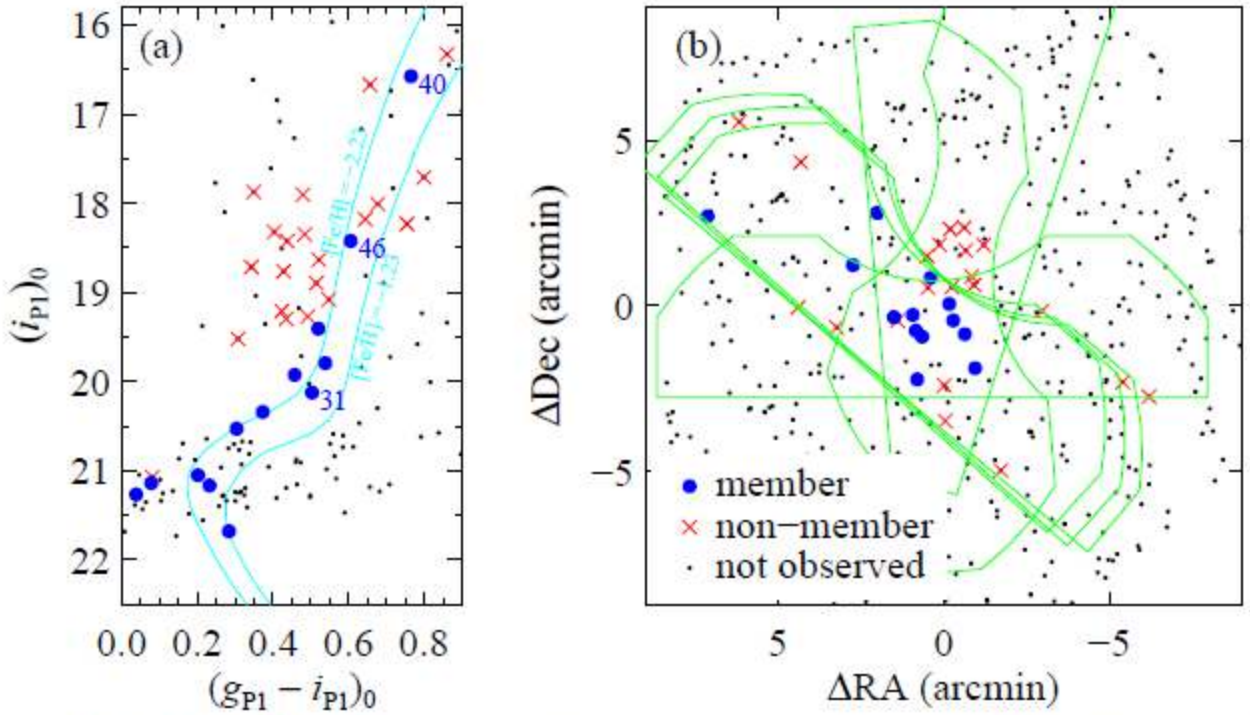

Figure 1. (*a*) CMD from Pan-STARRS photometry. Spectroscopic members are shown as large blue points, and non-members are red crosses. The cyan curves show 14 Gyr Padova isochrones (Girardi et al. 2004) at the distance of Tri II. The two isochrones have metallicities of [Fe/H] = −1.23 and −2.23. (*b*) The map of spectroscopic targets. The DEIMOS slitmask outlines are shown in green.

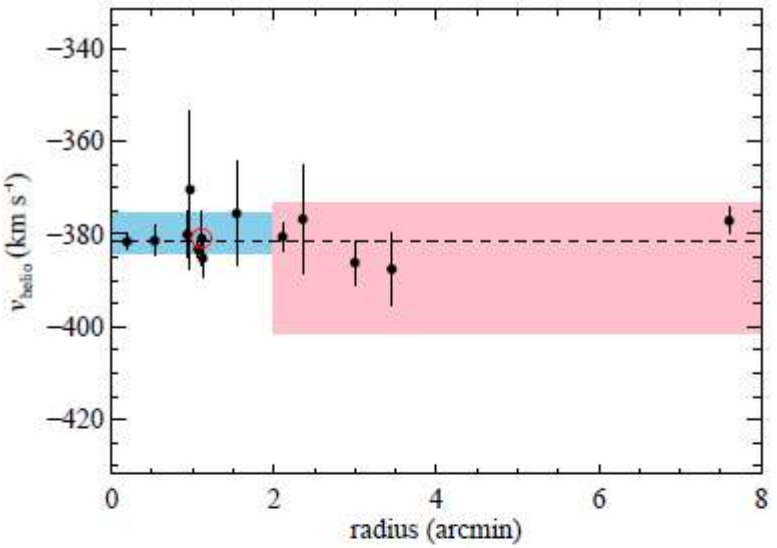

Figure 3. Radial velocity of Tri II members versus their distances from the center of the galaxy. The dashed line shows the mean velocity. The shaded regions show the velocity dispersions in different regions of the galaxy published by M16. The mean velocity of star 46, the binary, is indicated by a red circle. Our measurements do not show evidence for a velocity dispersion changing with radius.

Figure 4 shows the individual velocity measurements of the 12 member stars.
Each column is the velocity curve of a unique member star.
Thus, the binary orbital velocity of star 46 was driving the measurement of the velocity dispersion of Tri II rather than orbits in the galaxy's potential.

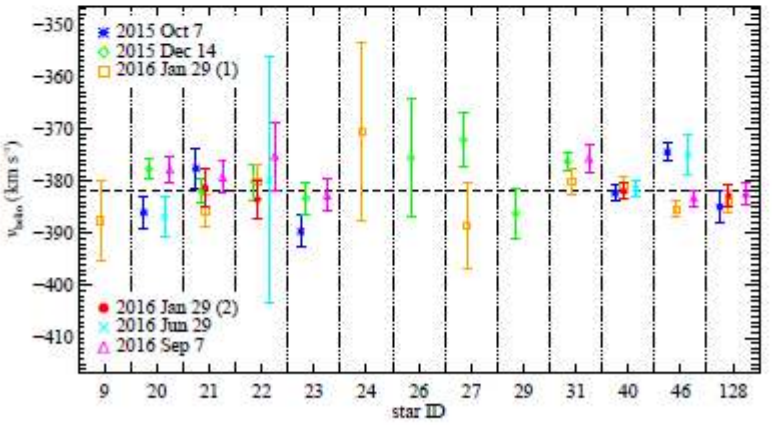

Figure 4. Heliocentric radial velocities observed at six different epochs. Each vertical column represents the measurements for one star. Within the column, the stars are ordered according to the date of observation. There are two independent measurements on 2016 Jan 26.

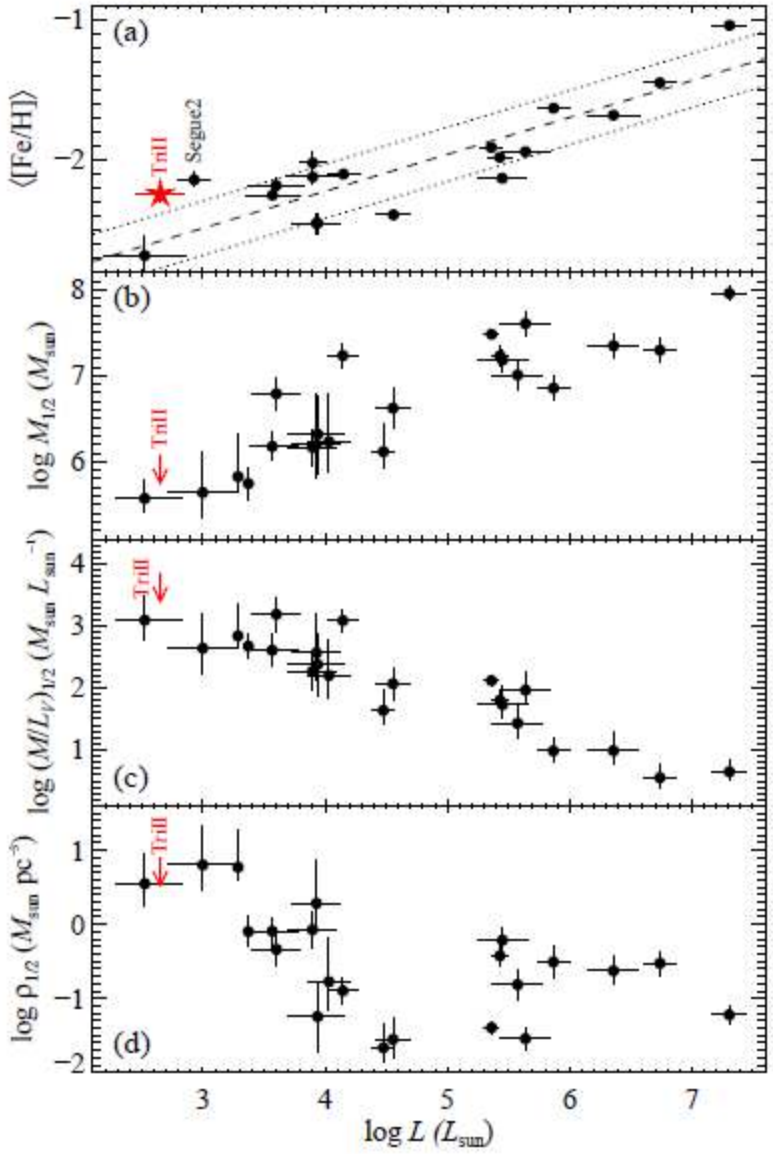

Figure 7. (*a*) Luminosity–metallicity relation. The dashed line shows the linear fit to the galaxies except Tri II (Kirby et al. 2013b, 2015b), and the dotted lines show the rms dispersion about the fit. (*b*) Masses of MW satellite galaxies within their 3D half-light radii assuming dynamical equilibrium. Data are from McConnachie

Основные выводы

- The galaxy lies above the mass–metallicity relation defined by Local Group dwarf galaxies. Both globular clusters and tidally stripped dwarf galaxies occupy this region of the mass–metallicity diagram. The upper limits on the kinematic properties of Tri II are consistent with dwarf galaxies, but they are also consistent with globular clusters, which have low mass-to-light ratios, like stellar populations free of dark matter.
- New mass limit indicates that Tri II does not have the largest mass-to-light ratio (M/L) of any non-disrupting galaxy (M/L_V <5000, if stable).
- Our high-resolution spectrum of the brightest known member star in Tri II shows exceptionally low abundances of Sr and Ba which is not typical for star clusters. It may very well be the strongest evidence in favor of classifying Tri II as a UFD rather than a star cluster.

A-ph 1703.03204

OMEGAWINGS: THE FIRST COMPLETE CENSUS OF POST STARBURST GALAXIES IN CLUSTERS IN THE LOCAL UNIVERSE

A. PACCAGNELLA[1,2], B. VULCANI[3], B. M. POGGIANTI[2], J. FRITZ[4], G. FASANO[2], A. MORETTI[2], Y. JAFFÉ[5], A. BIVIANO[6], M. GULLIEUSZIK[2], D. BETTONI[2], A. CAVA[7], W. COUCH[8], AND M. D'ONOFRIO[1,2]

[1]Department of Physics and Astronomy, University of Padova, Vicolo Osservatorio 3, 35122 Padova, Italy
[2]INAF - Astronomical Observatory of Padova, 35122 Padova, Italy
[3]School of Physics, University of Melbourne, VIC 3010, Australia
[4]Instituto de Radioastronomía y Astrofísica, IRyA, UNAM, Campus Morelia, A.P. 3-72, C.P. 58089, Mexico
[5]European Southern Observatory, Alonso de Cordova 3107, Vitacura, Casilla 19001, Santiago de Chile, Chile
[6]INAF - Astronomical Observatory of Trieste, 34143 Trieste, Italy
[7]Observatoire de Genève, Universitè de Genève, 51 Ch. des Maillettes, 1290 Versoix, Switzerland and
[8]Australian Astronomical Observatory, PO Box 915, North Ryde, NSW 1670 Australia

Draft version March 10, 2017

ABSTRACT

Galaxies that abruptly interrupt their star formation in < 1.5 Gyr present recognizable features in their spectra (no emission and Hδ in absorption) and are called post starburst (PSB) galaxies. By studying their stellar population properties and their location within the clusters, we obtain valuable insights on the physical processes responsible for star formation quenching. We present the first complete characterization of PSB galaxies in clusters at $0.04 < z < 0.07$, based on WINGS and OmegaWINGS data, and contrast their properties to those of passive (PAS) and emission line (EML) galaxies. For $V < 20$, PSBs represent $7.2 \pm 0.2\%$ of cluster galaxies within 1.2 virial radii. Their incidence slightly increases from the outskirts toward the cluster center and from the least toward the most luminous and massive clusters, defined in terms of X-ray luminosity and velocity dispersion. The phase-space analysis and velocity dispersion profile suggest that PSBs represent a combination of galaxies with different accretion histories. Moreover, PSBs with the strongest Hδ are consistent with being recently accreted. PSBs have stellar masses, magnitudes, colors and morphologies intermediate between PAS and EML galaxies, typical of a population in transition from being star forming to passive. Comparing the fraction of PSBs to the fraction of galaxies in transition on longer timescales, we estimate that the short timescale star-formation quenching channel contributes two times more than the long timescale one to the growth of the passive population. Processes like ram-pressure stripping and galaxy-galaxy interactions are more efficient than strangulation in affecting star formation.

TABLE 1
CLUSTER SAMPLE: GLOBAL PROPERTIES

Cluster	z	N_{mem}	σ_{cl} km s^{-1}	R_{200} Mpc	$\log(L_X)$ 10^{44} erg s^{-1}
A1069	0.0651	130	695 ±55	1.67	43.98
A151	0.0538	248	738 ±32	1.78	44.0
A1631a	0.0465	369	760 ±29	1.84	43.86
A168	0.0453	141	547 ±38	1.32	44.04
A193	0.0484	101	764 ±58	1.85	44.19
A2382	0.0639	322	698 ±30	1.67	43.96
A2399	0.0577	291	730 ±35	1.75	44.0
A2415	0.0578	194	690 ±38	1.66	44.23
A2457	0.0587	249	680 ±37	1.63	44.16
A2717	0.0498	135	544 ±47	1.32	44.0
A2734	0.0618	220	781 ±49	1.88	44.41
A3128	0.0603	480	839 ±29	2.02	44.33
A3158	0.0594	357	1024 ±37	2.46	44.73
A3266	0.0596	678	1319 ±40	3.17	44.79
A3376	0.0463	263	845 ±42	2.04	44.39
A3395	0.0507	369	1206 ±55	2.91	44.45
A3528	0.0545	262	1017 ±46	2.45	44.12
A3530	0.0549	275	674 ±39	1.62	43.94
A3556	0.048	359	669 ±35	1.62	43.97
A3558	0.0486	442	1003 ±34	2.42	44.8
A3560	0.0491	283	840 ±35	2.03	44.12
A3667	0.0558	386	1011 ±42	2.43	44.94
A3716	0.0457	327	849 ±27	2.05	44.0
A3809	0.0626	244	554 ±38	1.33	44.35
A3880	0.058	216	688 ±56	1.66	44.27
A4059	0.049	229	752 ±38	1.82	44.49
A500	0.0682	227	791 ±44	1.89	44.15
A754	0.0545	338	919 ±37	2.22	44.9
A85	0.0559	172	982 ±55	2.37	44.92
A957x	0.0451	92	640 ±47	1.55	43.89
A970	0.0589	214	844 ±49	2.03	44.18
IIZW108	0.0486	171	612 ±38	1.48	44.34

- While all PSB galaxies with strong H will later turn into PSBs with moderate H, the opposite is not true. Therefore, we will discuss also the strong PSB (Ha > 6 Å, hereafter sPSB) separately..
- EML = emission line galaxies.
- PAS= passive galaxies

TABLE 2
WEIGHTED SPECTRAL NUMBERS AND FRACTIONS

Galaxy type	PAS		PSB		sPSB		EML	
	N	%	N	%	N	%	N	%
Clusters	8162 (4235)	55.7±0.4	1057 (560)	7.2±0.2	154 (80)	1.1±0.3	5441 (3029)	37.0±0.4
Field	415 (225)	19.7±0.8	28 (15)	1.3±0.2	7 (3)	0.3±0.1	1667 (923)	79.0±0.9

NOTE. — Weighted Number (raw numbers in brackets) and percentage of the different spectral types for the magnitude-limited sample weighted for spectro
copic incompleteness and considering only galaxies inside $1.2R_{200}$. The field sample has no radial limits. The proportion of PAS (k), PSB (k+a/a+k), stron
SB (**the subsample of** PSB with EW(Hδ >=6) and EML galaxies are listed along with binomial errors.

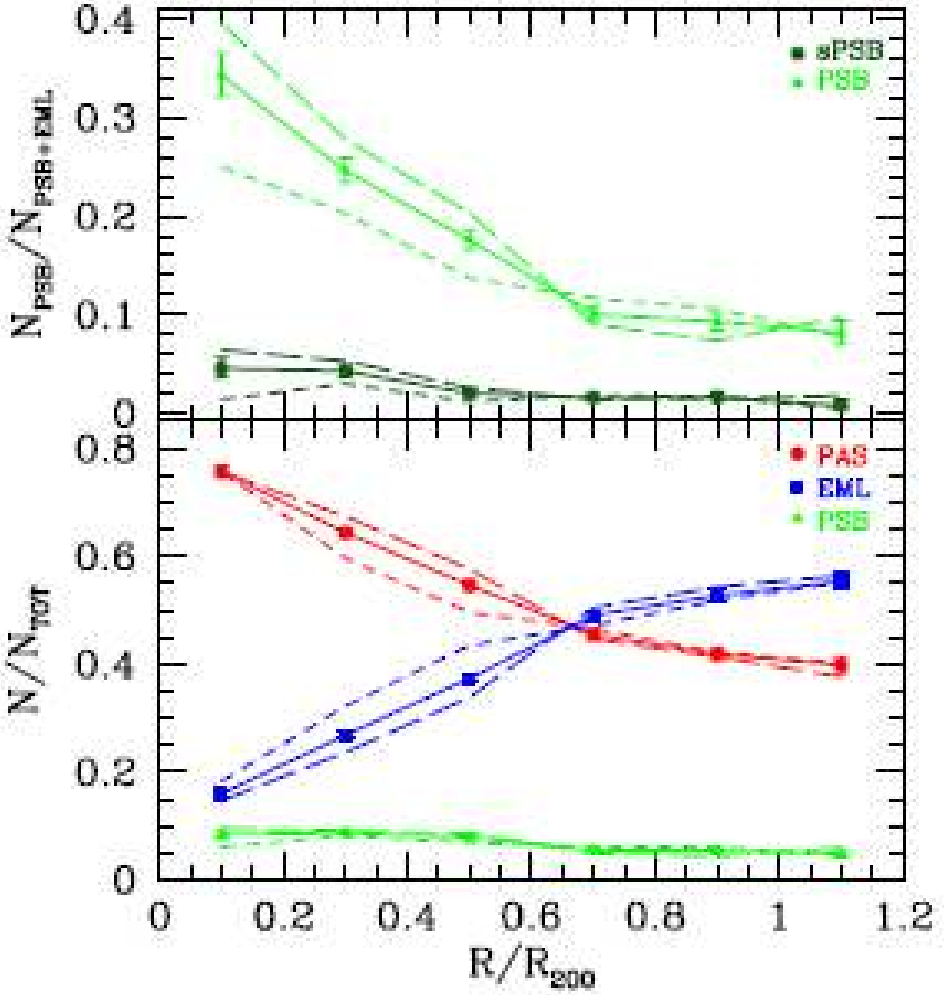

FIG. 4.— Ratio of post-starburst to active galaxies (top panels) and ratio of post-starburst, passive and emission line galaxies to the total (bottom panels) as a function of R/R_{200}. Points with error bars represent cluster fractions, dashed lines give the trends of the respective fractions in two bins of velocity dispersion σ ($\sigma < 840km/s$ -short dashed lines- and $\sigma > 840km/s$ -long dashed lines). Errors are binomial (Gehrels 1986).

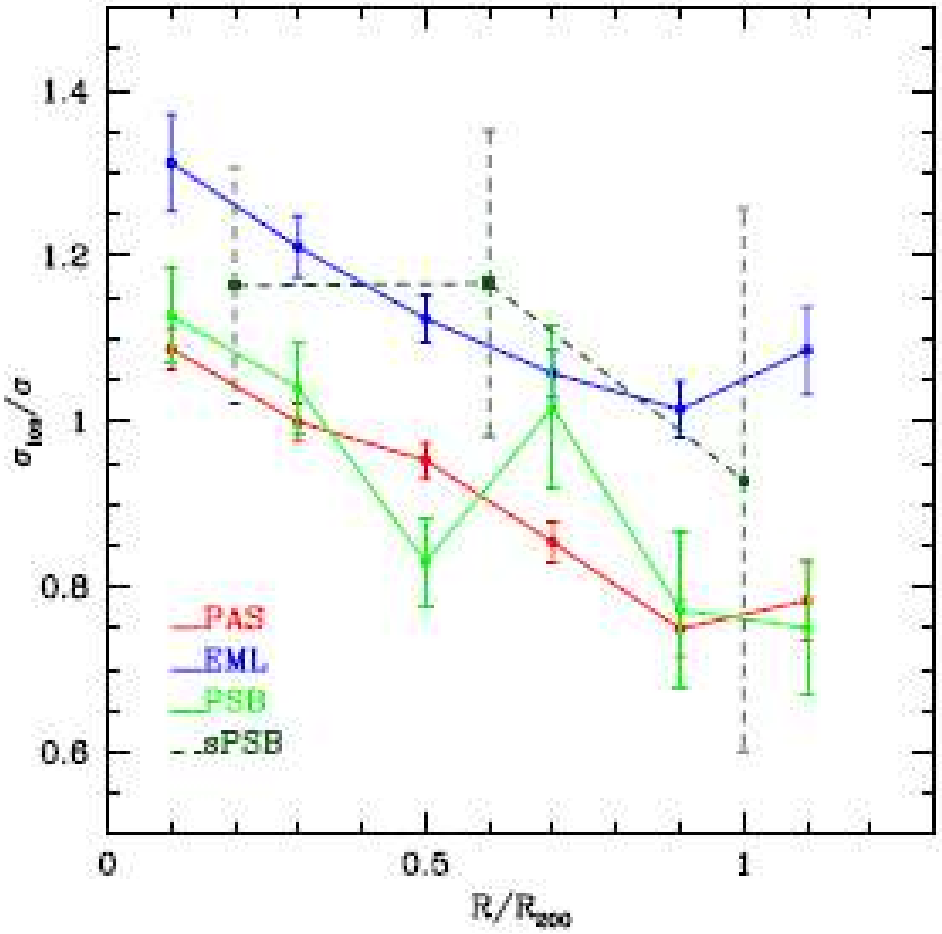

FIG. 6.— Velocity dispersion profiles ($\sigma_{LOS}(r)/\sigma$) of each galaxy population; colors refer to the different populations as described in the labels and as in Fig. 4. Errors are jackknife standard deviations (Efron 1982).

PSBs represent ~ 7% of cluster galaxies within 1.2 virial radii. Their incidence slightly increases from the outskirts toward the cluster center and from the least toward the most luminous and massive clusters, defined in terms of X-ray luminosity and velocity dispersion.

- The phase-space analysis and velocity dispersion profile suggest that PSBs represent a combination of galaxies with different accretion histories. PSBs with the strongest H are consistent with being recently accreted.
- PSBs have stellar masses, magnitudes, colors and morphologies intermediate between PAS and EML galaxies, typical of a population in transition from being star forming to passive.
- Comparing the fraction of PSBs to the fraction of galaxies in transition on longer timescales, we estimate that the short timescale star-formation quenching channel contributes two times more than the long timescale one to the growth of the passive population.
- Processes like ram-pressure stripping and galaxy-galaxy interactions are more efficient than strangulation in affecting star formation.